

joint chosen randomly from those not sampled in the previous sequence. All signal and noise dots were 7 arcmin in diameter, and were half-white and half-black against a grey background of 20 cd m<sup>-2</sup> (thus causing no change in mean luminance). The walker was generated by Cutting's algorithm<sup>7</sup> (with no net translation) from a randomly chosen starting position, usually at 0.75 gait-cycles per second, with the individual dots moving at an average speed of 1.8 deg s<sup>-1</sup>. For translation, dots were placed in random positions over the area of the walker, and all moved at 1.8 deg s<sup>-1</sup> (to obtain results shown in Fig. 2). The walker was symmetrical about the vertical midline (particularly the upper body), so spatial cues alone could not aid discrimination.

Observers fixated the centre of a Barco Calibrator monitor (frame rate 180 Hz) from a distance of 80 cm. After a warning signal, the target was presented to either the left or the right of fixation, with an appropriate density control on the other side (both stimuli subtended 3.4 × 5.7°, centred 2.4° from fixation). For the walker, the density control was derived from the walking algorithm by randomizing the order of the frames presented. For translation, the control dots were displayed in new random positions within the region on each frame. Thus both target and control were dynamic, but only in the target was the motion coherent and smooth. Detection of either class of stimuli could be based on a judgement of smoothness of motion of individual dots. Discrimination was a two-stage process, in which observers first selected which side contained the target, and then identified the direction of the moving dots (for translation), the direction of ambulation (for discrimination of biological motion), or whether the upper and lower body of the walker moved coherently. As the discrimination thresholds for translation were similar to those for detection, it is unlikely that the two-stage task was an impediment to performance.

Dynamic random noise, comprising dots of similar size and colour, was scattered over the entire screen. The density of the noise increased or decreased in each trial, depending on the correctness of the observer's response (following the adaptive procedure QUEST<sup>19</sup>, without feedback). There were 200–400 trials for each condition, with sensitivity defined as the noise level at which 75% correct responses are made; sensitivity was calculated by fitting a raised cumulative gaussian curve (with asymptotes at 0.5 and 1) to the psychometric functions. For spatial summation (Fig. 2), stimuli were presented for 1,200 ms (almost one complete gait-cycle, comprising 40 frames) centred within a noise window of 1,400 ms. For temporal summation (Fig. 3), the stimulus interval varied within a noise window of 7 s.

Received 12 June; accepted 21 September 1998.

- Johansson, G. Visual perception of biological motion and a model for its analysis. *Percept. Psychophys.* **14**, 201–211 (1973).
- Marey, E.-J. *Le Mouvement* (Masson, Paris, 1894).
- Mather, G. & Murdoch, L. Gender discrimination in biological motion displays based on dynamic cues. *Proc. R. Soc. Lond. B* **259**, 273–279 (1994).
- Dittrich, W. H., Troscianko, T., Lea, S. & Morgan, D. Perception of emotion from dynamic point-light displays represented in dance. *Perception* **25**, 727–738 (1996).
- Fox, R. & McDaniel, C. The perception of biological motion by human infants. *Science* **218**, 486–487 (1982).
- Morrone, M. C., Burr, D. C. & Vaina, L. Two stages of visual processing for radial and circular motion. *Nature* **376**, 507–509 (1995).
- Cutting, J. A program to generate synthetic walkers as dynamic point-light displays. *Behav. Res. Methods Instrument* **10**, 91–94 (1978).
- Watson, A. B. Probability summation over time. *Vision Res.* **19**, 515–522 (1979).
- Burr, D. C. Temporal summation over moving images by the human visual system. *Proc. R. Soc. Lond. B* **211**, 321–339 (1981).
- Green, D. M. & Swets, J. A. *Signal Detection Theory and Psychophysics* (Wiley, New York, 1966).
- Maloney, R. K., Mitchison, G. J. & Barlow, H. B. Limit to the detection of Glass patterns in the presence of noise. *J. Opt. Soc. Am. A* **4**, 2336–2341 (1987).
- Wilson, H. R., Wilkinson, F. & Asaad, W. Concentric orientation summation in human form vision. *Vision Res.* **37**, 2325–2330 (1997).
- Lappin, J. S. & Bell, H. H. The detection of coherence in moving random-dot patterns. *Vision Res.* **16**, 161–168 (1976).
- Barlow, H. B. & Tripathy, S. P. Correspondence noise and signal pooling in the detection of coherent visual motion. *J. Neurosci.* **17**, 7954–7966 (1997).
- Burr, D. C., Morrone, M. C. & Vaina, L. Large receptive fields for optic flow direction in humans. *Vision Res.* **38**, 1731–1743 (1998).
- Cutting, J. E. Coding theory adapted to gait perception. *J. Exp. Psychol.* **7**, 71–87 (1981).
- Marr, D. & Vaina, L. Representation and recognition of the movements of shapes. *Proc. R. Soc. Lond. B* **214**, 501–524 (1982).
- Ullman, S. in *Human and Machine Vision* (eds Beck, J., Hope, B. & Rosenfeld, A.) 459–480 (Academic, New York, 1983).
- Watson, A. B. & Pelli, D. G. QUEST: A Bayesian adaptive psychometric method. *Percept. Psychophys.* **33**, 113–120 (1983).
- Mather, G., Radford, K. & West, S. Low-level visual processing of biological motion. *Proc. R. Soc. Lond. B* **249**, 149–155 (1992).

**Acknowledgements.** We thank H. Barlow and J. Ross for useful discussions. P.N. was supported by a scholarship from the Scuola Normale Superiore, Pisa. Supported by MURST and EC BIOMED (VIPROM). Correspondence and request for materials should be addressed to D.C.B. (e-mail: daye@in.pi.cnr.it).

## Temporal dynamics of chromatic tuning in macaque primary visual cortex

Nicolas P. Cottaris\* & Russell L. De Valois†

\* Program in Vision Science and † Department of Psychology, University of California Berkeley, 3210 Tolman Hall, California 94720, USA

The ability to distinguish colour from intensity variations is a difficult computational problem for the visual system because each of the three cone photoreceptor types absorb all wavelengths of light, although their peak sensitivities are at relatively short (S cones), medium (M cones), or long (L cones) wavelengths. The first stage in colour processing is the comparison of the outputs of different cone types by spectrally opponent neurons in the retina and upstream in the lateral geniculate nucleus<sup>1–3</sup>. Some neurons receive opponent inputs from L and M cones, whereas others receive input from S cones opposed by combined signals from L and M cones. Here we report how the outputs of the L/M- and S-opponent geniculate cell types are combined in time at the next stage of colour processing, in the macaque primary visual cortex (V1). Some V1 neurons respond to a single chromatic region, with either a short (68–95 ms) or a longer (96–135 ms) latency, whereas others respond to two chromatic regions with a difference in latency of 20–30 ms. Across all types, short latency responses are mostly evoked by L/M-opponent inputs whereas longer latency responses are evoked mostly by S-opponent inputs. Furthermore, neurons with late S-cone inputs exhibit dynamic changes in the sharpness of their chromatic tuning over time. We propose that the sparse, S-opponent signal in the lateral geniculate nucleus is amplified in area V1, possibly through recurrent excitatory networks. This results in a delayed, sluggish cortical S-cone signal which is then integrated with L/M-opponent signals to rotate the lateral geniculate nucleus chromatic axes<sup>4–5</sup>.

The term 'receptive field' is used traditionally to characterize how a neuron responds to stimuli in different spatial locations, thus referring to a spatial receptive field<sup>6</sup>. Here we are concerned with determining how a cortical neuron responds to stimuli consisting of chromatic shifts from a white point to different locations in colour space, and how this responsiveness develops over time. We are therefore studying a chromatic–temporal receptive field. To examine the cortical transformation of lateral geniculate nucleus (LGN) chromatic signals directly, we specified stimulus chromaticity in the MacLeod–Boynton–Derrington–Krauskopf–Lennie (MBDKL) isoluminant plane<sup>7,8</sup>. This plane is defined by two axes whose chromaticities isolate responses from the two types of LGN opponent neuron<sup>8</sup>: the 0° to 180° axis isolates responses from L/M-opponent LGN neurons (0°: L – M, 'pinkish-red'; 180°: M – L, 'cyan'); and the 90° to 270° axis isolates responses from S-opponent LGN neurons (90°: S – (L + M), 'violet'; 270°: – S + (L + M), 'greenish-yellow'). A cortical cell that integrates signals from both types of colour-coding geniculate cell, as most cortical cells do, would have a preferred chromaticity at an intermediate angle, depending on the relative weights and timings of the cell's inputs.

To study the structure of the chromatic–temporal receptive field, we probed neurons with spatially uniform chromatic stimuli presented in a fast (30-ms flashes), pseudorandom sequence and analysed the neuronal response using the reverse-correlation procedure<sup>9,10</sup>. Stimulus dimensions were one to two times the classical receptive-field dimensions, as measured with *m*-sequence receptive-field mapping<sup>11</sup>. For each action potential (spike) fired, we determined which chromatic stimulus had been presented at various preceding times. Spikes were accumulated in a two-dimensional

**Table 1 Laminar distribution of cells**

Chromatic-temporal receptive field	2 + 3	4A/4B	4C <sub>α+β</sub>	5	6	Unknown	Total
Early, single-peaked	5	5	12	1	11	6	40
Late, single-peaked	11	3	4	4	3	0	25
Double-peaked	6	6	6	4	3	0	25
Continuously shifting	0	1	0	0	4	0	5
Cells per layer	22	15	22	9	21	6	95

Number of cells of various chromatic-temporal dynamics found in each cortical layer. More than half of the cells with early-peaking receptive fields were found in layers 4C and 6 and more than half of the cells with late-peaking receptive fields were found in the supragranular layers (2 + 3 and 4A/4B). Cells with double-peaked receptive fields were found in all layers. Almost all cells with continuously shifting receptive fields were found in layer 6.

histogram corresponding to stimulus chromaticity and time delay before spiking. After some thousands of spikes were processed this way, we found that, immediately before spiking, all stimuli were equally likely to have been presented as it takes around 30–50 ms for visual information to reach cortical area VI. However, for longer time delays, chromatic stimuli that excite the neuron would be more likely to have been presented, and those that inhibit the neuron would be less likely to have been presented.

The data set consists of 95 cells from 12 monkeys, all of which responded reliably and consistently to our rapidly changing stimulus (see Methods). About two-thirds of the cells showed a single chromatic preference over time, indicating that their different chromatic inputs all had similar temporal dynamics, whereas the remaining one-third of the cells exhibited major shifts in their colour tuning over time, reflecting multiple chromatic inputs with different latencies. Cells with a single chromatic peak appeared to fall into two classes on the basis of their latencies between stimulus presentation and spiking, namely those with early latencies (<96 ms) and those with longer latencies (≥96 ms). The validity of this division was reinforced by finding that these two classes differed also in their chromatic preferences and their chromatic-integration dynamics.

Neurons with early, single-peaked chromatic-temporal receptive fields (40 of 95) were found mainly in cortical layers 4C and 6 (Table 1). Their responses peaked between 68 and 96 ms after stimulus presentation (Fig. 1A), and they maintained a nearly constant sharpness of chromatic tuning during their response course (see below and Fig. 2), indicating static and instantaneous integration of their chromatic inputs. A smaller number of these neurons (3 of 40) had very short times-to-peak (55–70 ms), biphasic temporal impulse responses, strong inverted S-cone inputs (Fig. 1A, right-most receptive field) and were found in layer 6.

Neurons with late, single-peaked chromatic-temporal receptive fields (25 of 95) were found mainly in the supragranular layers (14 of 25). Their responses peaked between 96 and 135 ms after stimulus presentation and they had slower dynamics than the early-peaking neurons (Fig. 1B). In addition, the sharpness of chromatic tuning in most of these cells changed over time (Fig. 2c, inset), suggesting dynamic integration of their chromatic inputs. Almost all of these neurons had strong S-cone inputs with peak chromatic axes within 30° of the ±S geniculate axis.

Neurons with major shifts in their chromatic tuning over time were of two types, namely those with double-peaked receptive fields, exhibiting shifts of around 90° (25 of 95), and those exhibiting continuous 360° chromatic shifts (5 of 95). Most double-peaked neurons (22 of 25) responded first to stimuli around the L–M chromatic axis, followed 10–30 ms later by responses to stimuli around the S axis (Fig. 1Ca). The reverse configuration, early responses to S-stimuli and late responses to L/M-stimuli, was observed in 3 of 25 neurons (Fig. 1Cb). Double-peaked neurons were found in all layers. Neurons with continuously shifting receptive fields (Fig. 1D) started responding very early (40–50 ms after stimulus presentation), and had biphasic temporal impulse responses and significant S-cone inputs. Their chromatic-tuning sharpness at any point in time was nearly constant. Like the very

fast, biphasic neurons with strong inverted S-cone inputs (Fig. 1A, right-most receptive field; see above), these neurons were found mainly in layer 6 and may correspond to a postulated fast S-cone input to luminance<sup>12</sup> and motion-sensitive<sup>13</sup> mechanisms.

To quantify our results we extracted the time-to-peak of a cell's different chromatic responses by curve-fitting separate receptive-field time slices. Figure 3a shows the distribution of the time-to-peak parameter compiled across all chromaticities (grey histogram) and across chromaticities within ±30° from the L/M- and the S-opponent axes (red and purple histograms, respectively). The trough around 96 ms in the aggregate distribution indicates that there might be two major cortical chromatic-response types, those peaking before and those peaking after 96 ms (early and late responses, respectively). Furthermore, striate responses evoked by L/M-opponent inputs are fast (median 81 ms,  $\sigma = 7.1$  ms), comprising most of the early peak of the aggregate latency distribution, whereas responses evoked by signals from S-opponent inputs are slower (median 100 ms,  $\sigma = 16.9$  ms), contributing about one-third of the early portion and most of the late portion of the aggregate time-to-peak distribution. These data concur with visual-evoked-potential (VEP) measurements that show longer latencies in response to S-cone-isolating stimuli<sup>14</sup>, although the neural origin of the VEP signal is unknown.

Figure 3b illustrates the relationship between receptive-field peak chromaticity and receptive-field time-to-peak for neurons with single-peaked receptive fields. These parameters were extracted from fits of the entire receptive field (Methods). The preferred chromaticities of early-peaking neurons are distributed throughout most of the 360° chromatic range, with subtle gaps between the geniculate axes, whereas late-peaking neurons are mostly tuned near the ±S-cone axis. On the other hand, nearly all double-peaked neurons (Fig. 3c) have their early chromatic peaks in response to L/M inputs, and their delayed peaks in response to S inputs. This is further evidence for longer processing delays of S- versus L/M-opponent signals, and indicates that the integrated output of double-peaked neurons would have preferred chromaticities distributed between the L/M and S axes; these chromaticities are under-represented by neurons with single-peaked receptive fields.

The difference in processing delays of L/M- and S-opponent signals may originate precortically, as signals from the two cone-opponent systems are processed independently in the retina<sup>15</sup> and in the LGN<sup>8,16</sup>. However, electrophysiological results show that L/M- and S-opponent LGN neurons have nearly identical temporal dynamics<sup>17</sup>. Examination of the shape of chromatic tuning as a function of time gives further support for a cortical origin of the delayed, sluggish S-cone signal we have identified. Our stimuli produce sinusoidal variation in L-, M-, and S-cone contrasts as a function of chromatic angle, and parvocellular LGN neurons, which sum cone signals linearly, have sinusoidal chromatic tuning in this colour space<sup>8</sup>. However, cortical static nonlinearities, such as response threshold<sup>18</sup> and expansive relationships<sup>18,19</sup> between membrane potential and spike generation<sup>20</sup>, are expected to yield narrower chromatic tuning in cortical neurons. In addition, cortical recurrent, excitatory networks<sup>21</sup> could dynamically change the sharpness of chromatic tuning.

We studied the sharpness and the dynamics of sharpening of

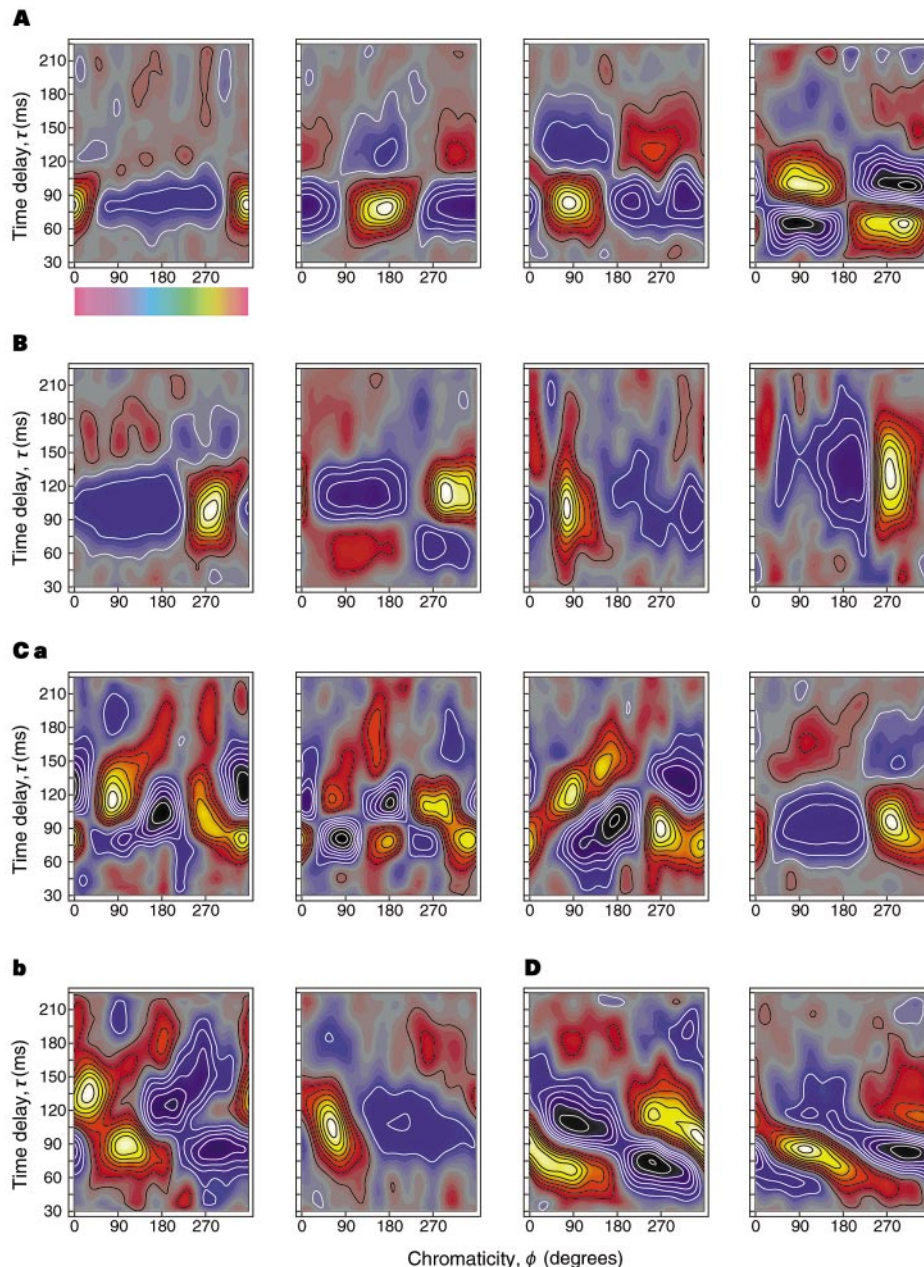


**Figure 1** V1 chromatic-temporal receptive-field maps. X-axis: stimulus chromaticity ( $0^{\circ}$  to  $360^{\circ}$ ). Y-axis: response delay. Response magnitude is colour-coded (see Methods). Colour bar approximates the colour of stimuli. **A**, Neurons with early, single-peaked receptive field. Times-to-peak (left to right): 82 ms, 77 ms, 82 ms, and 62 ms. **B**, Neurons with late, single-peaked receptive field. Times-to-

peak (left to right): 97 ms, 111 ms, 98 ms, and 132 ms. **C**, Neurons with double-peaked receptive field. **a**, Early L/M-opponent input with late S-opponent input. **b**, Rare neurons with early S-opponent input and late L/M-opponent input, respectively. **D**, Neurons with continuously shifting chromatic tuning.

cortical chromatic tuning by fitting receptive-field slices parallel to the chromatic axis at successive time intervals with exponentiated sinusoidal functions with a threshold (Methods). Response exponents close to 1 indicate linear summation of cone signals (LGN-like), with progressively larger exponents indicating progressively sharper tuning. The chromatic temporal receptive fields of 74 out of 95 neurons could be fitted adequately with such functions. It was found that neurons with stable, early-peaking receptive fields had narrower colour tuning than LGN cells (mean exponent at peak, 1.57). Most of these neurons (30 of 39) had stable exponents over time (Fig. 2a), with the remainder exhibiting only small dynamic changes, indicating static nonlinearities as the mechanism of response sharpening. Neurons with continuously shifting chromatic tuning also showed stable exponents over time (Fig. 2b) with extremely linear summation properties (mean exponent at

peak, 0.97). In contrast, late-peaking neurons were very sharply tuned (mean exponent at peak, 4.67), and 15 out of 19 showed large variations in their response exponents over time (Fig. 2c), indicating dynamic nonlinearities as the mechanism of response sharpening. All but one of these 15 neurons had primarily  $-S$  inputs. Changes in response exponent were also seen in the late, S-dominated peak in 9 out of 12 neurons with double-peaked receptive fields (Fig. 2d).

On the basis of these data, we propose that the relatively weak precortical S-cone signal (the signal is weak because of the sparse mosaic pattern of S cones<sup>22</sup> and S-opponent ganglion<sup>23</sup> and LGN<sup>6,24</sup> cells) is amplified in the cortex by a specialized mechanism, possibly a recurrent excitatory circuit in which the output of a striate neuron re-enters the cell to be summed synergistically with new signals. Lateral excitatory connections among proximal, S-dominated

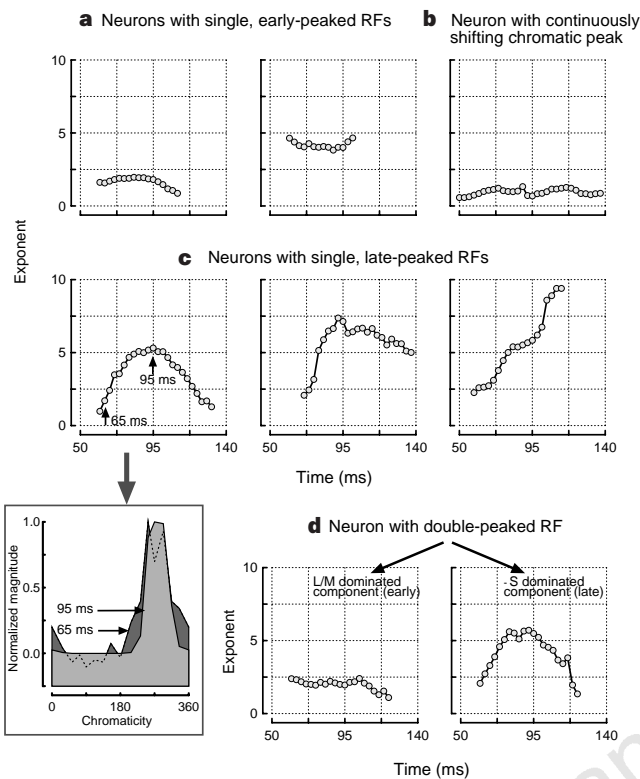


**Figure 2** Dynamics of sharpening of V1 chromatic responses. Response exponent is plotted as a function of time. **a, b**, Neurons with non-changing exponents. **c**, Neurons with late-peaked receptive fields (RFs). Inset: chromatic tuning profile at 65 ms (dark grey) and at 95 ms (light grey). **d**, Neuron with double-peaked RF. This neuron's RF was fitted with the sum of two components whose chromaticities fluctuated around 330° (L/M-dominated) and 265° (–S-dominated), which peaked at 80 ms and 98 ms, respectively. Of 33 neurons with dynamic changes in sharpness of chromatic tuning, the response exponent and response magnitude were correlated in 17. Response exponent increased or decreased continuously for 12 and 4 neurons respectively, of the remaining 16.

neurons may also contribute, as time-varying exponents, longer times-to-peak, and large S-cone responses are usually seen at very low spatial frequencies (N.P.C. and R.L.D.V., manuscript in preparation). The resulting S-cone signal is quite different from that seen in the LGN, having longer latency and slower dynamics, dynamically modified sharpness over time, and equal representation of both polarities (–S cells are extremely rare in the retina and the LGN<sup>24,25</sup>). This amplified, but sluggish, cortical S-cone signal becomes integrated with the abundant LGN L/M-opponent signal, rotating the LGN chromatic axes to form the perceptual 'red–green' and 'blue–yellow' colour axes<sup>5</sup>. This arrangement places a constraint in the minimal integration window needed by next-order neurons for the reliable sampling of signals from double-peaked neurons. Such integration windows would be of the order of 40–90 ms for signals from double-peaked neurons, contrasting with the 20–30-ms windows for signals from single-peaked neurons. This cortical amplification and nonlinear processing of the S-cone information concurs with recent psychophysical results<sup>26</sup>. □

**Methods**

Rhesus monkeys (*Macaca mulatta*) were tranquilized with ketamine HCl (10–15 mg kg<sup>-1</sup>, intramuscular). Anaesthesia was maintained with a continuous intravenous (i.v.) infusion of sufentanil citrate (5–12 µg kg<sup>-1</sup> h<sup>-1</sup>, i.v.). Electrocardiogram, electroencephalogram, body temperature and expired CO<sub>2</sub> were continuously monitored. All the procedures were in accord with NIH guidelines and approved by the University of California Animal Care and

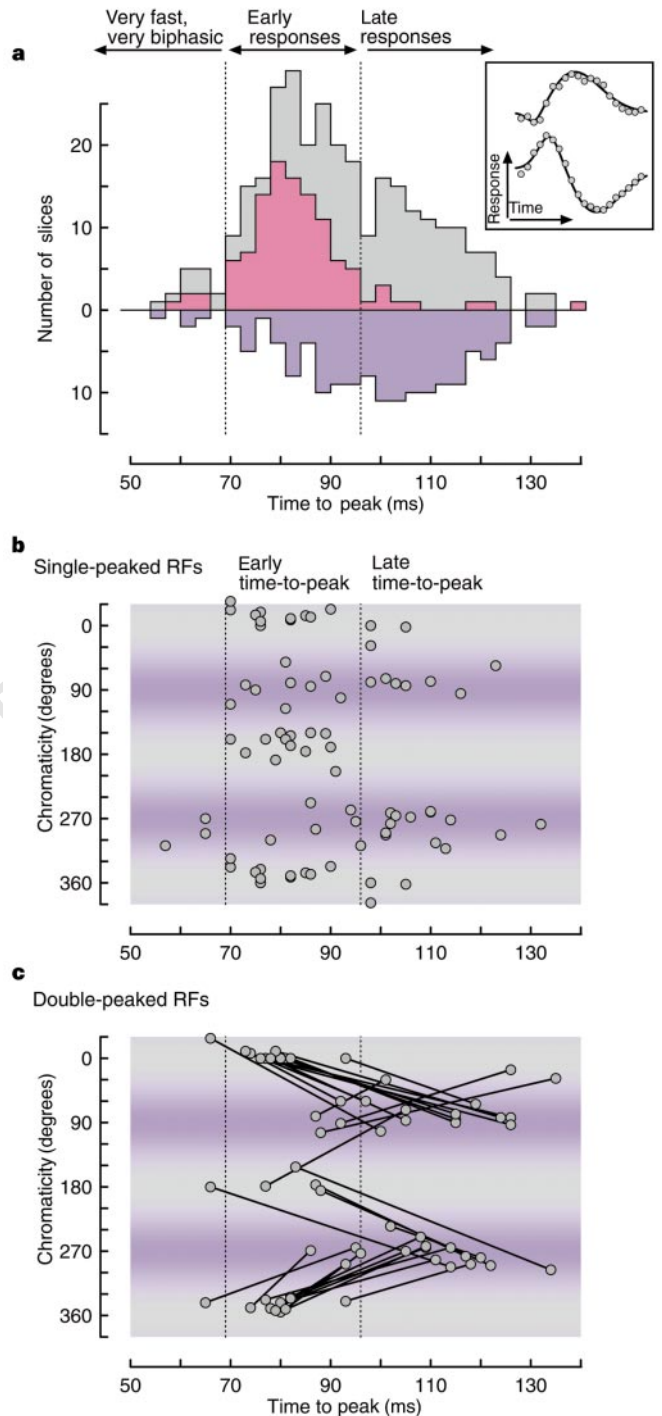


**Figure 3** Times-to-peak of V1 chromatic responses. **a**, Distributions of times-to-peak extracted by curve fitting of separate receptive-field slices parallel to the time axis (see Methods). Grey, aggregate distribution compiled across all chromaticities (315 responses from 95 neurons); red and purple, distributions for slices taken at chromaticities within ±30° of the L–M and the S axes, respectively. Inset shows typical curve fits. **b**, Neurons with single-peaked receptive fields (RFs). RF peak chromaticity is plotted against its time-to-peak (see Methods). **c**, Neurons with double-peaked RFs. Each cell's characteristic 90° chromatic transition is sampled at two points (RF regions of peak response) and the points are connected to identify individual cells. Grey–purple grating in **b, c** depicts S-cone contrast variation.

Use Committee. Visual stimuli were generated by a SUN/TAAC-1 image processor, and displayed on an NEC monitor with a 66-Hz refresh rate and a mean luminance of 70 cd m<sup>-2</sup>. Receptive fields were located within the central 5°. Action potentials were recorded with 1-ms resolution. Small lesions (5–10 µA × 5 s) were made every 500 µm along the length of each penetration.

Reconstruction of penetrations and assignment of cells to cortical layers was done using published criteria<sup>27</sup>.

**Colour space.** Chromatic tuning was measured in the isoluminant plane of the three-dimensional MBDKL colour space<sup>7,8</sup>, at chromaticity angles,  $\phi$ , of 0°, 28°, 53°, 73°, 90°, 112°, 135°, 157°, 180°, 208°, 233°, 253°, 270°, 292°, 315° and 337°, with an achromatic adaptation point (Illuminant C). On this circle, the L-, M- and S-cone contrasts were sinusoidal functions of chromaticity with maximum attainable values of 8%, 16% and 83%, respectively.

**Cell selection.** Only cells with consistent receptive fields in successive stimulation blocks were included in the data set. All included cells had receptive fields with a signal-to-noise (S/N) ratio of at least +22 dB. The S/N ratio was calculated as the ratio of the power (sum of squares) of the receptive field at the optimal delay (signal) to the power of the receptive field at zero delay (noise). Nearly all cells in the data set gave chromatic responses that were equally strong or stronger than their responses to a spatially uniform, 20% contrast, achromatic stimulus.

**Chromatic-temporal receptive-field visualization.** Chromatic-temporal receptive-field maps were computed on a 16 × 40 grid and subsequently interpolated and smoothed. Magnitude of firing probability is colour-coded: grey corresponds to random, uncorrelated firing; warm colours (red to yellow to white) correspond to progressively higher-than-random firing probability; cool colours (light blue to dark blue to black) correspond to progressively lower-than-random firing probability. Iso-response contours are drawn at intervals of 6.25% correlation level.

**Curve fitting.** To extract times-to-peak (in separate receptive field slices), receptive-field slices parallel to the time axis ( $\tau$ ) were fit with a function that describes a damped oscillation,  $F(\tau): F(\tau) = A \times \text{Env}(\tau, \tau_p; \tau_r; \tau_d) \times \text{Sin}(2\pi \times (f \times \tau - \xi/360))$ , with

$$\text{Env}(\tau, \tau_p; \tau_r; \tau_d) = \begin{cases} e^{-0.5 \left( \frac{\tau - \tau_p}{\tau_r} \right)^2}, & \tau \leq \tau_p \\ e^{-0.5 \left( \frac{\tau - \tau_p}{\tau_d} \right)^2}, & \tau > \tau_p \end{cases}$$

where  $A$  is the response gain,  $\tau_p$  is the envelope's peak latency,  $\tau_r$  and  $\tau_d$  are time constants for the rising and decaying phases of the damping envelope, respectively, and  $f$  and  $\xi$  are the temporal frequency and temporal phase of the oscillation, respectively. The slice's time-to-peak was extracted by searching for the  $\tau$  value for which  $F(\tau)$  reached its maximum. Separate receptive-field slice fitting was done to extract time-to-peak values for all chromatic temporal receptive fields, including those whose unusual structure (90° chromatic shifts) precluded fitting of the entire receptive field, and to extract a more complete set of time-to-peak values for all the different chromaticities tested. For single-peaked chromatic-temporal receptive fields (Fig. 1A, B) three slices were fit, corresponding to the three chromaticities of maximum response. For double-peaked receptive fields (Fig. 1C), six slices were fit, three around each chromatic peak. For cells with continuously changing responses latencies (Fig. 1D), three slices were fit around their first strong peak.

To extract receptive-field peak chromaticity, receptive-field time-to-peak, and response exponent (entire receptive-field fit), receptive-field slices parallel to the chromaticity axis ( $\phi$ ) were taken at successive time intervals ( $\tau_i$ ) throughout the cell's entire response duration and fit with a function,  $G(\phi, \tau_i)$ , that describes an exponentiated sinusoid with a threshold:  $G(\phi, \tau_i) = A(\tau_i) \times \text{Max}\{\text{Sgn}(f(\phi, \tau_i)) \times |f(\phi, \tau_i)|^{n(\tau_i)}, T\}$ ,  $\tau_i = 0, 4, \dots, 220$  ms, with

$$f(\phi, \tau_i) = \text{Sin}(2\pi \times (\phi - \phi(\tau_i))/360), \quad \text{Sgn}(x) = \begin{cases} +1, & x \geq 0 \\ -1, & x < 0 \end{cases}$$

where  $A(\tau_i)$ ,  $n(\tau_i)$  and  $\phi(\tau_i)$  are the response gain, the response exponent, and the chromatic axis of the receptive field, respectively, at a stimulus-response delay of  $\tau_i$  ms, and  $T$  is the response threshold ( $T = 0$  for half-wave rectified responses). For neurons with relatively constant chromatic preference, receptive-field peak chromaticity was obtained by averaging  $\phi(\tau_i)$  over a time window in which  $A(\tau_i)$  was within 80% of its maximum value. Receptive-field time-to-peak was obtained by finding the  $\tau_i$  value for which  $A(\tau_i)$  reached its maximum.

Received 22 June; accepted 20 August 1998.

- De Valois, R. L. *et al.* Analysis of response patterns of LGN cells. *J. Opt. Soc. Am.* **56**, 966–977 (1966).
- Lennie, P. & D'Zmura, M. Mechanisms of color vision. *CRC Crit. Rev. Neurobiol.* **3**, 333–400 (1988).
- Dacey, D. Circuitry for color coding in the primate retina. *Proc. Natl Acad. Sci. USA* **93**, 582–585 (1996).

- Lennie, P. *et al.* Chromatic mechanisms in striate cortex of macaque. *J. Neurosci.* **10**, 649–669 (1990).
- De Valois, R. L. & De Valois, K. K. A multi stage color model. *Vision Res.* **33**, 1053–1065 (1993).
- Hartline, H. K. The receptive fields of optic nerve fibers. *Am. J. Physiol.* **130**, 690–699 (1940).
- MacLeod, D. I. A. & Boynton, R. M. Chromaticity diagram showing cone excitation by stimuli of equal luminance. *J. Opt. Soc. Am.* **69**, 1183–1186 (1979).
- Derrington, A. M. *et al.* Chromatic mechanisms in the lateral geniculate nucleus of macaque. *J. Physiol. (Lond.)* **357**, 241–265 (1984).
- de Boer, E. & Kuyper, P. Triggered correlation. *IEEE Trans. Biomed. Eng.* **15**, 169–179 (1968).
- Ringach, D. L. *et al.* Dynamics of orientation tuning in macaque primary visual cortex. *Nature* **387**, 281–284 (1997).
- Reid, R. C. *et al.* The use of m-sequences in the analysis of visual neurons: linear receptive field properties. *Vis. Neurosci.* **14**, 1015–1027 (1997).
- Stockman, A. *et al.* The temporal properties of the human short-wave photoreceptors and their associated pathways. *Vision Res.* **31**, 189–208 (1991).
- Gegenfurtner, K. R. & Hawken, M. J. Temporal and chromatic properties of motion mechanisms. *Vision Res.* **35**, 1547–1563 (1995).
- Rabin, J. *et al.* Visual evoked potentials in three-dimensional color space: correlates of spatio-chromatic processing. *Vision Res.* **34**, 2657–2671 (1994).
- Dacey, D. M. & Lee, B. B. The 'blue-on' opponent pathways in primate retina originates from a distinct bistratified ganglion cell. *Nature* **367**, 731–735 (1994).
- Martin, P. R. *et al.* Evidence that blue-on cells are part of the third geniculocortical pathway in primates. *Eur. J. Neurosci.* **9**, 1536–1541 (1997).
- Gielen, C. C. A. M. *et al.* Reconstruction of cone-system contributions to responses of colour-opponent neurons in monkey lateral geniculate. *Biol. Cybern.* **44**, 211–221 (1982).
- Tolhurst, D. J. & Heeger, D. J. Comparison of contrast-normalization and threshold models of the responses of simple cells in cat striate cortex. *Vis. Neurosci.* **14**, 293–309 (1997).
- Albrecht, D. G. & Geisler, W. S. Motion selectivity and the contrast-response function of simple cells in the visual cortex. *Vision Res.* **7**, 531–546 (1991).
- McCormick, D. A. *et al.* Comparative electrophysiology of pyramidal and sparsely spiny stellate neurons of the neocortex. *J. Neurophys.* **54**, 782–806 (1985).
- Pugh, M. *et al.* Computational modeling of orientation tuning dynamics in V1 neurons. *Soc. Neurosci. Abstr.* **23**, 603 (1997).
- de Monasterio, F. M. *et al.* Staining of blue-sensitive cones of the macaque retina by a fluorescent dye. *Science* **213**, 1278–1281 (1981).
- Calkins, D. J. *et al.* Microcircuitry and mosaic of a blue-yellow ganglion cell in the primate retina. *J. Neurosci.* **18**, 3373–3385 (1998).
- Malpeli, J. G. & Schiller, P. H. Lack of blue off-center cells in the visual system of the monkey. *Brain Res.* **141**, 385–389 (1978).
- Lennie, P. Recent developments in the physiology of color vision. *Trends Neurosci.* **5**, 243–248 (1984).
- De Valois, R. L. *et al.* Color appearance with and without S-opponent cells. *Vision Res.* (submitted).
- Hawken, M. J. *et al.* Laminar organization and contrast sensitivity of direction-selective cells in the striate cortex of the old world monkey. *J. Neurosci.* **8**, 3541–3548 (1988).

**Acknowledgements.** We thank K. K. De Valois, S. D. Elfar, J. Gallant and E. Switkes for comments on the manuscript, and E. Switkes for implementation of the MBDKL colour space. This work was funded by the NIH.

Correspondence and requests for materials should be addressed to N.P.C. (e-mail: nicolas@valois.berkeley.edu).

## Selective activation of Ca<sup>2+</sup>-activated K<sup>+</sup> channels by co-localized Ca<sup>2+</sup> channels in hippocampal neurons

Neil V. Marrion & Steven J. Tavalin

Vollum Institute, Oregon Health Sciences University Portland, Oregon 97201, USA

Department of Pharmacology, School of Medical Sciences, University of Bristol, Bristol BS8 1TD, UK

Calcium entry through voltage-gated calcium channels can activate either large- (BK) or small- (SK) conductance calcium-activated potassium channels. In hippocampal neurons, activation of BK channels underlies the falling phase of an action potential and generation of the fast afterhyperpolarization (AHP)<sup>1,2</sup>. In contrast, SK channel activation underlies generation of the slow AHP after a burst of action potentials<sup>3</sup>. The source of calcium for BK channel activation is unknown, but the slow AHP is blocked by dihydropyridine antagonists<sup>4,5</sup>, indicating that L-type calcium channels provide the calcium for activation of SK channels. It is not understood how this specialized coupling between calcium and potassium channels is achieved. Here we study channel activity in cell-attached patches from hippocampal neurons and report a unique specificity of coupling. L-type channels activate SK channels only, without activating BK chan-